Pressure measurement in gas flows using laser-induced grating lifetime

CHRISTOPHER WILLMAN[1], LAURENT M. LE PAGE[1], PAUL EWART[2], AND BENJAMIN A. O. WILLIAMS[1,*]

[1] Dept. Engineering Science, University of Oxford, UK
[2] Dept. Physics, University of Oxford, UK
[*] Corresponding author: ben.williams@eng.ox.ac.uk

Compiled April 6, 2021

Optical diagnostics of gas-phase pressure are relatively unusual. In this work we demonstrate a novel, rapid and robust method to use laser-induced grating scattering (LIGS) to derive this property in real time. Previous pressure measurements with LIGS have employed a signal fitting methodology but this is relatively time consuming and requires specialist understanding. In this paper, we directly measure a decay lifetime from a LIGS signal and then employ a calibration surface constructed using a physics-based model to convert this value to pressure. This methodology was applied to an optically-accessible single cylinder internal combustion engine, yielding an accuracy of better than 10 % at all tested conditions above atmospheric pressure. This new approach complements the existing strength of LIGS in precisely and accurately deriving temperature with a simple analysis method, by adding pressure information with a similarly simple method.

http://dx.doi.org/10.1364/ao.XX.XXXXXX

1. INTRODUCTION

Pressure is an important metric in a wide variety of gaseous flow systems and is conventionally measured using transducers embedded in the wall of a vessel or chamber. These typically provide robust and accurate measurements of the local pressure at the wall surface which for many purposes is an effective representation of the bulk pressure. For applications requiring high spatial resolution of surface pressure gradients, pressure-sensitive paint provides a spatially resolved alternative to discrete transducers [1]. There are however many situations where spatial variation or rapid fluctuations in pressure away from the walls is of interest such as high-speed wind tunnels, shock tubes and internal combustion engines [2–4]. In such environments it is either undesirable or impractical to disturb the flow with an intruding physical probe. Non-invasive optical techniques provide remote measurement of pressure within the flow, enabling studies of localised pressure variations within flow fields such as those associated with auto-ignition leading to damaging 'knock' in internal combustion engines.

Several optical methods exist for remote measurement of pressure in gases that provide both temporal and spatial resolution. Various approaches have been used to estimate the pressure fields associated with particle-imaging velocimetry (PIV) measurements of flow fields. One such method to utilise snapshot PIV data to infer instantaneous pressure information uses Taylor's hypothesis. A study by Van der Kindere et al.[5] used this approach to approximate pressure distribution in separated and re-attaching flows within 4 % of the dynamic pressure transducer measurement (≈ 2 Pa). An alternative method for obtaining pressure from PIV data uses an Eulerian and Lagrangian approach performed by De Kat et al.[6], which was also verified using surface-transducer pressure data for validation. In their work, the pressure at the side-wall and base of a square cylinder could be determined from PIV data with a difference with respect to the pressure transducers of 5 % and 2 %, respectively [6]. PIV inherently lends itself to 2D measurements with planar illumination of particles either naturally present in or, more often, seeded into the flow. Sequential 2D measurements may then be stacked to give an averaged 3D result, such as the 3D pressure and velocity fields in the vicinity of a propeller tip [7]. Time-resolved volumetric pressure fields may be evaluated from tomographic PIV using volume illumination and multiple simultaneous camera views [8, 9].

Both temporally and spatially resolved measurements have also been performed using non-linear optical techniques such as coherent anti-Stokes Raman scattering (CARS) [10–13]. Simultaneous temperature and pressure measurements have been made using dual-pump CARS in a gas cell covering the range 0.1 atm to 20 atm with a mean absolute error of less than 8 % [14]. Hybrid fs/ps CARS in nitrogen where the collisional environment is well known has shown accuracies of 7.5 % or better for pressures of 0.4 atm to 3 atm by exploiting the increased pressure-sensitivity of long pulse delays at the expense of several orders of magnitude of signal intensity [11]. The upper pressure limit

of this approach is expected to be of order 5 atm to 10 atm due to the need for collision-free thermometry at short probe delays as a precursor to the pressure derivation. Dual-probe hybrid fs/ps rotational CARS for simultaneous single-shot temperature, pressure, and O_2/N_2 ratio has recently been demonstrated for temporally resolved one-dimensional measurements [15]. Accuracies of < 1 % and precisions from 0.83 % to 2.44 % were achieved for pressures close to atmospheric from 1 bar to 1.5 bar.

A less complex non-linear technique that does not require fitting to a spectrally-resolved signal is laser-induced grating scattering (LIGS), also known as laser-induced thermal acoustics (LITA) [16–18]. LIGS/LITA experiments measure the speed of sound in a gas directly and models of the LIGS signal evolution can be used to determine transport properties such as the acoustic damping rate and thermal diffusivity, of key interest for studies of fundamental fluid physics [19]. Previous studies have demonstrated the capabilities of the LIGS technique for temperature measurements, which can readily achieve sub-1 % precision and accuracies of order 1 % [20–24]. Under ideal conditions of high pressure (10 bar) and a binary mixture of known gases (NO_2 and N_2) this can improve to an accuracy of 0.42 % and precision of 0.16 % [25].

In this work, we focus instead on the recovery of pressure information using the LIGS technique. Pressure measurements using LIGS have been made in a gas cell held at constant pressures, with an overall accuracy of 5.7 % and precision of 1.4 % achieved over a range of 3 bar to 40 bar [25]. When applying LIGS to a high pressure flame, measurements exhibited single-shot precisions of the order of 10 %, with a pressure-dependent accuracy of 7 % and 22 % for 40 bar and 20 bar respectively [26].

The accuracy of LIGS pressure measurements typically diminishes with decreasing total pressure as the signals become shorter. An alternative method utilising the downstream transport of counter-propagating acoustic wave packets in supersonic flows does enable an accuracy of 4 % for very low pressures, 0.06 bar to 0.14 bar, however it cannot be applied to subsonic flows [27]. The present work focuses on measurements made at an intermediate range of pressures from 0.5 bar to 6.5 bar, in an optically accessible gasoline direct injection (GDI) internal combustion engine, for which a recent extension of the model fitting approach for LIGS analysis presented accuracies of better than 10 % and precisions between 4 % to 10 % for measurement of motored in-cylinder pressures between 1 bar to 6.5 bar [28].

In this work a novel and rapid method of evaluating the decay lifetime of an acquired LIGS signal and then using a calibration surface to recover a pressure measurement is presented. The accuracy and precision of pressure recovery is evaluated over the range 0.5 bar to 6.5 bar and compared to the model fitting method of Sahlberg et al. [28]. This signal lifetime approach has the potential to permit real-time data processing for spatially and temporally resolved remote pressure measurements in dynamic environments using LIGS.

2. LASER-INDUCED GRATING SCATTERING

Laser-induced grating scattering (LIGS) is a four-wave mixing technique based on opto-acoustic effects that arise from the interference of two crossed pulsed laser beams. The principles of LIGS are well described in the literature [17, 29, 30] and only a brief summary is provided here.

A typical LIGS experiment is arranged using two parallel polarised pump laser beams from the same laser source, crossed at an angle, θ. The overlapped beams generate an interference pattern within the crossing volume, with fringe spacing, Λ, determined by the crossing angle and the laser wavelength, λ,

$$\Lambda = \frac{\lambda/2}{\sin(\theta/2)} \tag{1}$$

The interaction of the light field in this interference pattern with the medium arises from two possible mechanisms, resonant absorption and electrostriction. The first mechanism, resonant absorption, produces excitation of molecular energy levels and subsequent relaxation processes lead to thermal energy being transferred to the bulk medium and, consequently, to a temperature and density perturbation in the form of the interference pattern. This perturbation results in a spatially-periodic modulation of the refractive index in the form of a grating, referred to hereafter as a thermal grating. The second mechanism, electrostriction, leads to a similar refractive index grating as a result of spatial modulation of the density and the grating, in this case, is referred to as an electrostrictive grating. In both cases the rapid perturbation of the density launches two counter-propagating acoustic waves which establish a standing acoustic wave. In the first case, the temperature perturbation provides a stationary grating and the standing acoustic wave, so that scattering of a probe beam from the grating creates a signal beam in the process referred to as Laser-induced Thermal Grating Scattering, LITGS. In the second case, the grating arises only from the standing acoustic wave and is called Laser-induced Electrostrictive Grating Scattering, LIEGS. In the case of LITGS, the acoustic standing wave oscillates in and out of phase with the stationary component of the thermal grating. As a result, the modulation depth, and hence the scattering efficiency, of the grating oscillates periodically at a frequency, f, that is determined by the local sound speed, c_s, at which the acoustic waves traverse the grating spacing, Λ. For a probe beam incident at the appropriate Bragg angle, θ_B,

$$\theta_B = \sin^{-1}\frac{\lambda}{2\Lambda} \tag{2}$$

to the grating, the intensity of the scattered signal beam is proportional to the scattering efficiency of the grating. The LITGS signal therefore oscillates at the frequency, f, given by,

$$f = \frac{c_s}{\Lambda} = 2\frac{c_s}{\lambda}\sin\frac{\theta}{2} \tag{3}$$

The stationary thermal and oscillating acoustic components of the overall density perturbation, and consequently the grating, decay over time due to thermal diffusion and viscous damping.

The temporal profile of the LITGS signal may be recorded and used to derive the local temperature and pressure within the probed measurement volume. Under ideal gas conditions, temperature, T, is related to the oscillation frequency of the signal, f, via

$$T = f^2\Lambda^2\frac{m}{\gamma k_B} \tag{4}$$

where m is the mean molecular mass of the gas mixture, γ is the ratio of specific heats, and k_B is Boltzmann's constant. Pressure influences the rate of decay of the signal, allowing the local pressure within the medium to be evaluated via the methods discussed in Section 4.

In absorbing media the LITGS signal usually dominates, typically being several orders of magnitude stronger than the concurrent LIEGS signal. In this work toluene is used as an absorbing

component within the fuel-air mixtures so that all LIGS data presented here can be considered to arise from LITGS signals.

Deriving a temperature measurement from the temporal oscillations of a LIGS signal therefore relies on accurately determining the oscillation frequency, which is typically achieved by locating the dominant peak in the power spectrum of a LIGS signal [31, 32].

3. EXPERIMENTAL ARRANGEMENT

A. LIGS apparatus

The laser-induced grating was created by the interference of two pump pulses from a frequency-quadrupled Nd:YAG laser (Continuum Minilite II) produced by splitting the output beam at a 50 % beam splitter. Each pump pulse at 266 nm had an energy of 2 mJ and a duration of 5 ns. The CW probe beam at 660 nm, with a continuous power of up to 750 mW, was provided by the output of a diode-pumped solid state laser (Laser Quantum Ventus 660).

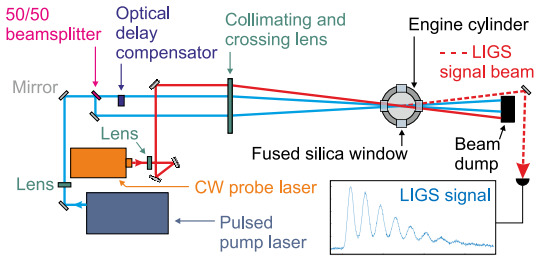

Fig. 1. LIGS system optical layout.

The pump and probe beams were directed through opposing fused silica windows at the top of the cylinder, intersecting at its centre. The measurement volume had an effective length of approximately 10 mm and a width of 1 mm as defined by the intersection of the two pump beams at an angle of 2.0° in a forward folded BOXCARS arrangement [33]. Lenses placed upstream of the crossing lens in each beam path ensured the pump and probe beams were collimated at the crossing point with diameters of $\sim$ 1 mm via a telescope arrangement. The oscillating component of the LITGS signal decays both by decay of the refractive index grating as a result of dissipative relaxation processes and by transit of the acoustic waves out of the interaction region. The use of comparatively large collimated beams, as opposed to focused beams with a waist of order 100 µm, minimises the decay of signal oscillations resulting from the transit of the acoustic perturbation. Maximising the number of recorded signal oscillations in this way is beneficial for accurate determination of the oscillation frequency and subsequently temperature.

Bragg-scattering of the probe beam off the formed grating generates the signal beam with a time varying intensity. The beam-like signal is spectrally filtered to remove scattered light from the pump beams and directed to a photomultiplier tube-based photosensor module (Hamamatsu H10721) with a rise time of <1 ns. The detected signal is then digitised using a fast digital oscilloscope (LeCroy Waverunner 625Zi) having a bandwidth of 2.5 GHz and a sampling rate of 20 giga-samples per second.

B. Optical engine

For this study, LITGS signals were generated in fuel/air mixtures inside an optically accessible single-cylinder engine, based on a Jaguar Land Rover gasoline direct injection (GDI) engine. Motoring this engine provided conditions of varying pressure and temperature with which to develop the LIGS pressure measurement technique. The cylinder has a bore of 85 mm and a stroke of 90.3 mm and its combustion chamber geometry includes a pent-roof with two intake and two exhaust valves. Just below the cylinder head, a removable steel annulus with inset 26 mm clear aperture fused silica windows forms the upper section of the cylinder. The optical engine was run at an approximately constant motored engine speed of 800 rpm with a compression ratio of 12.5:1. The experiments of this work only consider motored operation in which the pressure and temperature variation of the in-cylinder mixture is due to compression and expansion as a result of the externally driven piston motion, without combustion.

Toluene acted as the absorbing species for the LIGS pump beams, added to the non-absorbing base fuel, iso-octane, to give a concentration of 30 % toluene by volume. The fuel was injected via a centrally mounted fuel injector at 280° before top-dead-centre (bTDC) in order to provide a nominally homogeneous, stoichiometric fuel-air mixture during late compression [34]. The resulting toluene number density of approximately 0.5 % is sufficiently low to minimise any laser-induced perturbation in local temperature and pressure, due to energy absorption from the pump beams, while providing sufficient signal intensity [35].

A data acquisition and synchronisation system was used to control the LIGS system timing for engine measurements. In-cylinder pressures were measured with a water-cooled Kistler 6041A pressure transducer mounted within the cylinder head and were recorded at a rate of one sample per crank angle degree (°CA) using a National Instruments PCI-M10-16E-1 card. All pressures in this work, whether derived from transducer measurements or LIGS signals, are presented as absolute pressures.

4. LIGS PRESSURE MEASUREMENT METHODS

LITGS signals are transient events in which a temperature and density perturbation is rapidly formed (in approximately 10 ns) due to energy deposition by the pump beams, resulting in a modulation in the refractive index, the grating, which gradually dissipates, returning to a locally homogeneous environment. The dissipation rate is affected by changes in the thermal and mass diffusivities of the gas with temperature and pressure. For constant temperature, the signal decay lifetime increases with increasing pressure owing to the decrease in thermal and mass diffusivities. This presents an opportunity to measure pressure using LIGS signals by evaluating the duration or decay lifetime of the signal. While measuring the signal lifetime is , in concept, straightforward, conversion of the lifetime to pressure requires further thought.

A. Model-fitting method (MFM)

One approach for deriving pressure measurement from LIGS signals is the model-fitting method (MFM) outlined by Sahlberg et al. which finds the best fit for a modelled LIGS signal to the experimental data, then extracts the pressure values from the fit parameters [28]. A brief summary is provided here.

The evolution of the spatially-periodic modulation of the refractive index (grating) is modelled using the solution to the linearised hydrodynamic equations derived from the principles of conservation of mass, momentum and energy [16, 26]. The MFM implements the Fourier domain approach of Stevens and Ewart [25] which incorporates quenching processes occurring on

multiple time scales. The solution is a function of five parameters which encompass the relevant geometric and thermodynamic properties of the refractive index perturbation and the energy deposition process.

The grating evolution may be characterised in terms of the Reynolds number, Re, and the inter-fringe transit time, τ_g, defined as the time taken for the acoustic waves to traverse between fringes and given by τ_g. For LITGS signals, τ_g also corresponds to the time period of the oscillations in scattered signal intensity. The electronic excitation of the absorbing/tracer molecules transfers energy locally to the bulk gas via many possible multi-stage collisional quenching pathways. These may be collectively represented by two nominal quenching processes: one 'fast' process with rate, Q_1, and one 'slow' process with rate, Q_2 [28]. The relative contribution of each process is described by the branching ratio, r, defined as the fraction decaying via the slow pathway.

The values of these five parameters which provide the best fit to an experimental signal may then be used to extract properties of interest. Of relevance to this work is the Reynolds number, Re, which when combined with the ideal gas equation of state gives an expression for pressure,

$$p = \frac{\mu k_B T \mathrm{Re}}{c_s \Lambda m} \tag{5}$$

where k_B is the Boltzmann constant. Temperature, T, and sound speed, c_s may be measured directly from the oscillations in the LIGS signal via Equations 3 and 4. The mean molecular mass, m, and the viscosity, μ, may be evaluated using knowledge of the gas composition.

Allowing five parameters to vary in a fitting process is unlikely to produce a single optimal value for each parameter. To mitigate this, the model fitting method utilises a multi-step fitting method in which initial educated guesses of the five parameter values are iteratively improved by attempting to isolate their influence on specific parts of the LIGS signal. While this is a successful approach, achieving accuracies of better than 10 % for pressures above 1 bar, a consequence of the multiple fitting stages is a long processing time per signal of approximately 4 seconds. This prevents the MFM approach being applicable to real-time processing at typical pump laser repetition rates. These issues of complexity and slow processing rate provide motivation for a faster, more direct approach - the signal lifetime method.

B. Signal lifetime method

In contrast to the computationally-intensive multi-parameter fitting of the MFM approach, the signal lifetime method is designed to directly and rapidly extract the pressure-dependent decay lifetime of a LIGS signal and then convert it to pressure via a calibration surface. This potentially enables real-time readout of pressure at the expense of requiring preliminary measurements to build the calibration surface.

Extracting the decay lifetime from an acquired LIGS signal is achieved by firstly determining the signal's oscillation frequency by locating the dominant peak in the power spectrum. The oscillations of the signal may then be suppressed by smoothing using a moving average filter with a window size that is equal to the oscillation period. This isolates the contribution to the LIGS signal intensity arising from the stationary component of the grating. The evolution in time of this oscillation-suppressed LIGS signal may be approximated by an exponential decay (Equation 8).

Deviations from this exponential decay occur at the beginning of the signal (high intensity), due to the finite rate of grating formation via quenching effects, and at its end (low intensity) where the signal intensity approaches the baseline noise level. If included, both these early and late signal contributions tend to perturb the average slope of the signal to smaller magnitude (shallower) values. Upper and lower intensity thresholds of 80 % and 20 % of the signal's peak intensity were selected, maximising the gradient magnitude derived from various sample LIGS signals, in order to determine the valid region of decay.

Having established fixed thresholds to define the valid pressure-calculation region of the LIGS signals, the natural logarithm of each smoothed signal is taken and the resulting gradient, m_{fit}, is evaluated by a linear fit. The decay lifetime of the LIGS signal, τ_{signal}, can then be defined as

$$\tau_{\mathrm{signal}} = \frac{-1}{m_{\mathrm{fit}}} \tag{6}$$

increasing with increasing pressure but requiring translation via a calibration surface to recover absolute pressure. An illustration of this process is shown in Figure 2.

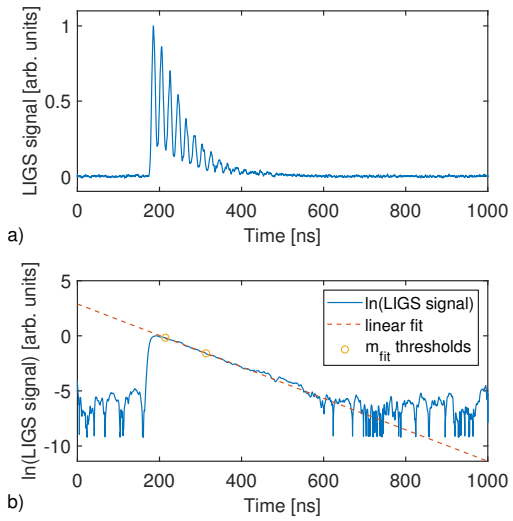

Fig. 2. Example of signal decay lifetime recovery. a) An example single-shot LIGS signal at 2.78 bar and 375.7 K. b) Illustration of the calculation of m_{fit} from a linear fit (red dashed line) to the natural logarithm of the example signal of a) (blue line) between threshold values (yellow circles) defined to avoid the deviations from exponential decay at the start and end of a LIGS signal.

Complicating this analysis is the fact that the signal decay lifetime depends not only on pressure, but also on composition (including associated changes in quenching rates), and on temperature. An increase in temperature leads to faster thermal diffusion, which results in a more rapid decay of the grating and therefore signal intensity. For a given gas composition, the calibration surface must therefore cover the range of both pressures and temperatures encountered during a measurement campaign.

The simplest approach to generate an empirical calibration surface is to fit an arbitrary (e.g. polynomial) relationship between pressure, temperature and signal decay lifetime values derived from LIGS signals under known conditions. This is likely to generate good estimates of pressure when applied to 'unknown' LIGS signals at conditions between the 'known' calibration points. However, achieving a sufficient density of cali-

bration conditions to accurately recover pressures may be costly in terms of time and requires prior knowledge of the calibration conditions over the entire range of relevant pressures and temperatures (or simultaneous measurement with an independent technique). Being a simple polynomial fit, it will also be highly unreliable to extrapolate beyond the calibration conditions and will require a fresh calibration surface to be generated for each new experimental setup.

A better approach is instead to consider a physics-based model of the pressure and temperature dependence of the signal decay lifetime. Being underpinned by the relevant physics of the processes involved, such a calibration surface may be more resilient to extrapolation and application to multiple experimental setups using just a single range of calibration conditions.

C. Pressure recovery

In an attempt to physically evaluate what shape the surface of decay lifetime as a function of p and T would take, expressions developed by Paul et al. that describe the temporal evolution of the grating signal were considered [16, 36, 37]. Paul et al. states that there is a contribution to the laser-induced grating from both a stationary temperature modulation and the standing acoustic wave. However, in the processing of the signal to estimate the decay lifetime, the signal oscillations are filtered out of the data (discussed in Section B), leaving only the contribution from the stationary thermal component, which is expressed as

$$\text{Signal}_{\text{st}} \propto \left[\exp\left(\frac{-(2\pi)^2 c_s t}{\text{RePr}\Lambda}\right)\right]^2 \tag{7}$$

and is dependent on the Reynolds number, $Re = \frac{c_s \Lambda \rho_0}{\mu}$, where ρ_0 is the probed medium density, and the Prandtl number, $Pr = \frac{c_p \mu}{k}$. Note that the expression is squared in order to represent a scattering efficiency rather than a refractive index variation. By analogy with Equation 6, this exponentially decaying signal contribution may be expressed as

$$\text{Signal}_{\text{st}} \propto \exp\left(\frac{-t}{\tau_{\text{signal}}}\right) \tag{8}$$

with a time constant, τ_{signal}, equivalent to the measured signal decay lifetime of the oscillation-suppressed LIGS signal (Equation 6) and given by

$$\tau_{\text{signal}} = \frac{\text{RePr}\Lambda}{2(2\pi)^2 c_s} = \frac{c_s \Lambda^2 \rho_0 c_p \mu}{2(2\pi)^2 c_s \mu k} = \frac{\Lambda^2 \rho_0 c_p}{2(2\pi)^2 k} \tag{9}$$

However, it is not known how τ_{signal} varies with both pressure and temperature. Examining parameters in Equation 9, some informed assumptions can be made. For example, the fringe spacing, Λ, is a constant and the probed medium density can be obtained from the ideal gas law

$$\rho_0 = \frac{p}{RT} \tag{10}$$

where R is the specific gas constant. The specific heat at constant pressure, c_p, is a function of temperature, although its value for air varies by only about 5 % when considering an increase from 300 K to 600 K, which is comparable to the range of temperatures observed in motored engine operation. Thermal conductivity, k, is also a function of temperature but not pressure. Tabulated values for nitrogen at 300 K and 600 K nearly double from approximately 26 mW/mK to 45 mW/mK, respectively [38–41]. Theory suggests that this variation scales as $T^{0.5}$ but observations have found the variation to scale faster, around $T^{0.75}$ at these considered temperatures [42, 43].

As pressure tends towards zero, the decay lifetime of an experimentally-measured LIGS signal cannot tend to zero due to the finite duration of the pump pulses and the finite detector bandwidth. The signal decay lifetime is therefore assumed to consist of both a constant term and a term that, neglecting the variation in c_p over the range of motored temperatures, depends on pressure and temperature as a result of variations in density and thermal conductivity. We model the signal lifetime by the following expression,

$$\tau_{\text{signal}} = A + B\left(\frac{p}{T^C}\right) \tag{11}$$

where A, B and C are unknown constants to be determined empirically and the temperature exponent, C, is expected to have a value within the range $1 < C < 2$.

5. RESULTS

LIGS measurements were performed during motored operation of the optical engine to satisfy two objectives.

Firstly, in order to determine the values of the A, B and C coefficients of Equation 11 and hence generate a calibration surface relating the LIGS signal decay lifetime to pressure and temperature, LIGS signals were recorded during the compression stroke of the motored optical engine between 90° and 40° bTDC for various inlet conditions. The accuracy and precision of pressure recovery using this calibration surface, compared to pressure transducer measurements, was evaluated using LIGS signals recorded under conditions of pressure and temperature *within* the range spanned by the calibration datasets.

Secondly, the applicability of the signal lifetime method to LIGS signals obtained with a) a different optical geometry and b) spanning a wider range of pressures and temperatures to that of the calibration surface was investigated. This permitted a) testing of the ability to transfer the calibration surface between instruments and b) investigation of the reliability of the calibration when extrapolated.

A. Calibration surface generation and evaluation

During the compression stroke, pressure and temperature vary as a function of crank angle following a polytropic process. Under 'baseline' inlet conditions of 1 bar and 20°C, mean temperatures each derived from sets of 50 LIGS signals recorded in increments of 10°CA between 90° and 40° bTDC are displayed as blue circles in Figure 3 against the corresponding pressure transducer measurements. By also varying the inlet temperature (20°C to 60°C) and pressure (1 bar to 1.16 bar) between datasets, LIGS signals covering a range of pressures (1.8 bar to 7.6 bar) and temperatures (343 K to 497 K) were obtained (Figure 3).

The three datasets of Figure 3 represent the extrema of the intake conditions of this work, being a 'standard' intake at atmospheric pressure and a temperature of 20 °C, a 'high temperature' intake heated to 60 °C and at atmospheric pressure, and a 'high pressure' intake raised to approximately 1.16 bar while maintained at a temperature of 20 °C. These datasets were used to construct a three-dimensional calibration surface that relates in-cylinder pressure transducer measurements, LIGS signal decay lifetimes and LIGS derived temperatures.

The values of the A and B coefficients of Equation 11 were determined by allowing the exponent, C of T, to vary from 1 to 2 in an increment of 0.01, and taking the difference between

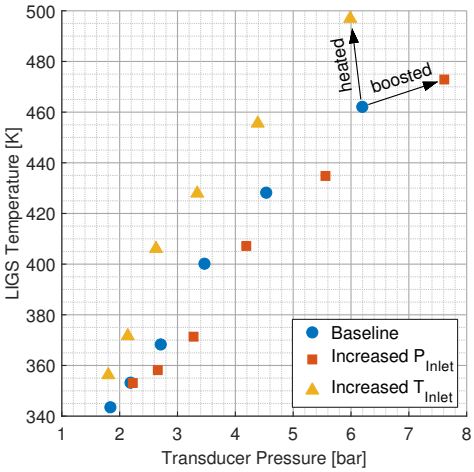

Fig. 3. LIGS temperature as a function of transducer pressure for three calibration datasets covering 'baseline' (1 bar, 20°C), 'heated' (1 bar, 60°C) and 'boosted' (1.16 bar, 20°C) inlet conditions. Each datapoint corresponds to the mean of temperatures derived from 50 LIGS signals at a fixed crank angle during the compression stroke.

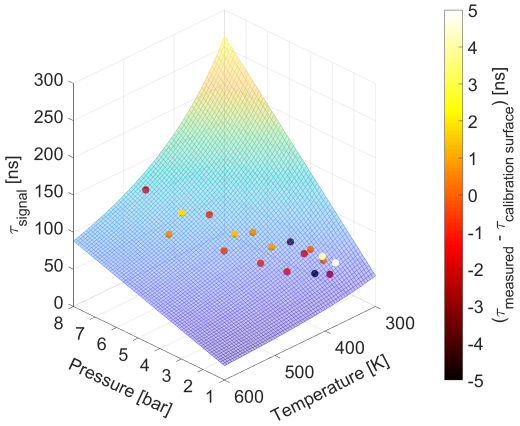

Fig. 4. Calibration surface relating transducer pressure, LIGS temperature and LIGS signal decay lifetime. Filled circles represent the datapoints of Figure 3 used for generating this calibration surface. The colour of each circle, as detailed in the colour bar, shows the difference in signal decay lifetime between each datapoint and the corresponding point on the calibration surface with the same pressure and temperature.

the resulting estimate of τ_{signal} using the transducer pressure data and τ_{signal} measured directly from the LIGS signal. An optimal value of 1.70 was found for the temperature exponent, C. The corresponding A coefficient was 9.42×10^{-9} s and the B coefficient (evaluated for pressure in bar and temperature in Kelvin) was 5.19×10^{-4} s.

Figure 4 displays the calibration surface obtained via Equation 11 using the best fit values of the A, B and C coefficients. The shape of the surface is constrained by the physical relationship between the parameters and provides a good match to the calibration data (filled circles). All calibration datapoints lie within 5.1 ns of the calibration surface, with an RMS error in τ_{signal} of 2.4 ns, or 3.1 % of the mean τ_{signal}. Reducing the number of calibration points reduces the investment in time, experimental effort and the number of known conditions required to generate a given calibration surface at the expense of accuracy. Using only the extremal 3 datapoints of highest temperature, highest pressure and lowest temperature doubles the RMS error in pressure of the surface from 0.11 bar (18 datapoints) to 0.21 bar (3 datapoints).

To quantify the accuracy of pressure recovery using this calibration surface, pressures derived from LIGS signals were compared to transducer pressure measurements for datasets at different intake conditions to those included in the calibration procedure. Figure 5 illustrates the transducer pressures and LIGS temperatures of the 'test' data (red squares) whose conditions lie within the bounds of the 'calibration' data (blue circles).

The error in the LIGS pressure measurement, defined as the difference to the corresponding transducer pressure measurement, is shown in Figure 6 as a function of signal to noise ratio (SNR). LIGS derived pressure measurements are sorted by the SNR of the LIGS signal, then divided into groups of 75 to show the trend in mean error and standard deviation of LIGS pressures. For the SNR calculation, the 'signal' is defined as the maximum value of the LIGS signal, typically the height of the first peak of the oscillating waveform. The 'noise' was estimated using the difference between the maximum and minimum values of the the last 5 % of the signal, which represents the worst-case variation in signal baseline after the LIGS signal was no longer present.

Within the range of pressures and temperatures spanned by the calibration conditions, the LIGS pressure measurements of Figure 6 are insensitive to the SNR of the LIGS signal. The LIGS pressures are well centred around the pressure transducer values, with a mean error of −0.5 %. While the mean pressure derived from LIGS is not strongly affected by SNR, the variation in derived pressure is increased for SNR below 10 (standard deviations from 9.7 % to 17.1 %) compared to SNR above 10 (standard deviations from 5.6 % to 8.8 %).

The error in LIGS derived pressure as a function of transducer pressure is shown in Figure 7. Similarly to Figure 6, LIGS pressure measurements are sorted by the corresponding transducer pressures and divided into groups of 75. The horizontal trend and mean error of −0.5 % are consistent with the error in LIGS measurement being independent of transducer pressure. The increased variation apparent for the lower pressures, below 2.3 bar, is in part due the lower SNR earlier in the compression stroke as the larger in-cylinder volume corresponds to a lower number density of the toluene tracer, resulting in weaker LIGS signals.

Sources of error in LIGS measurements, common to many coherent beam techniques, include fluctuations in intensity of the incident lasers, changes in local gas composition, beam steering and window fouling which may lead to uncertainties in the measurements of temperature and pressure. The LIGS technique, however, is distinguished from a range of established intensity-based diagnostics because the temperature is derived from a measurement of the frequency of signal oscillations rather than intensity. Thus, temperature measurement with LIGS is inherently more robust to errors arising from factors that affect the signal intensity. Measurement of the signal decay lifetime relies on the relative rate of change of signal intensity over the duration of the signal, rather than an absolute value. Pressure measurement with LIGS therefore also has some inherent re-

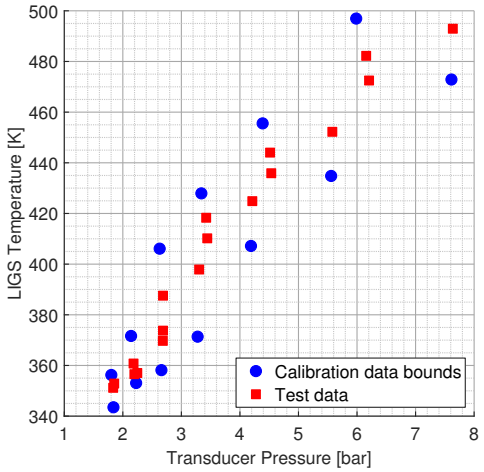

Fig. 5. Experimental conditions under which LIGS signals were recorded. Blue circles represent the bounds of the pressure and temperature range of the calibration data, cf. Figure 3. Red squares represent the pressure and temperature conditions of the 'test' data used to evaluate the performance of the calibration surface of Figure 4. Each datapoint corresponds to the mean of temperatures derived from 50 LIGS signals at a fixed crank angle during the compression stroke.

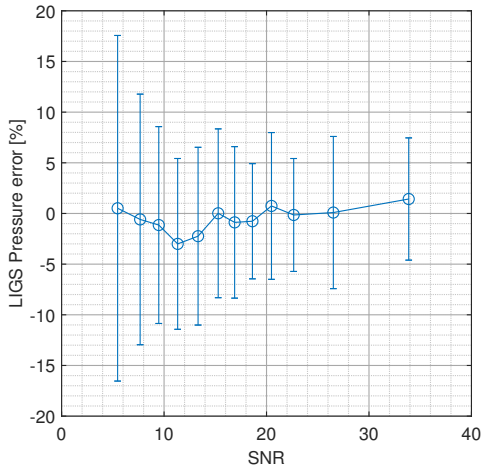

Fig. 6. Percentage errors of pressures derived from LIGS compared to signal-to-noise ratio (SNR). The LIGS 'test data' of Figure 5 is sorted by SNR and divided into groups of 75 LIGS signals. Each datapoint represents the mean error and mean SNR for the 75 LIGS signals within a group, with errorbars corresponding to the standard deviation.

silience to signal intensity fluctuations, provided they occur on timescales longer than the duration of the LIGS signal, for this work > 1 µs.

Variations in local gas composition will contribute to the variability of the LIGS pressure measurements by affecting the measurement of both temperature (Equation 4) and τ_{signal} (Equation 9). Without time-resolved knowledge of the composition fluctuations at the measurement location, the gas composition for each recorded LIGS signal must be assumed constant and equal to the composition used to derive the calibration surface. Considering a representative upper limit of 23 % variation in fuel number density at the measurement location, as measured previously under similar conditions to this work [34], the estimated uncertainty in derived pressure due to gas composition is 3 % at 3.5 bar and 400 K.

B. Calibration surface applicability

It is relatively straightforward to generate a self consistent calibration surface for a particular experimental set-up, but such a calibration surface is in general not globally applicable to other experiments. The utility of the calibration procedure demonstrated in Section A is greatly improved if it is possible to apply the calibration surface to LIGS signals collected using a range of experimental set-ups utilising the same LIGS tracer species.

To test the wider applicability of the calibration surface derived in Section A (Figure 4), a previously acquired LIGS dataset used to demonstrate the Model Fitting Method for LIGS pressure recovery in Sahlberg et al. [28] was investigated, enabling a direct comparison between the two pressure recovery methods. While broadly similar to the setup described in Section 3, the LIGS optical layout used a different probe laser and pump crossing angle, θ, resulting in a different LIGS grating spacing, Λ. This dataset of LIGS measurements was obtained using a modified piston with a rectangular slot to allow the transmission of the pump and probe beams when the piston was at top-dead-centre, enabling measurements to be made for a full 360°CA covering the entire compression and expansion strokes. The range of pressures and temperatures covered within this dataset is therefore greater than those of the calibration measurements of Section A.

In this work, a single known point of reference at atmospheric pressure has been found to be a suitable way to rescale the calibration surface to accommodate changes in geometry and so on. In effect, this results in a modification of the B coefficient of Equation 11. Figure 8 presents the results of applying the calibration surface of Figure 4 re-scaled to match the pressure transducer reading at the single reference point of 80° bTDC (0.94 bar). The LIGS pressures show very good agreement with the transducer pressures, even near TDC where recorded pressures of over 6 bar are far from the re-scaling reference value of 0.94 bar. The majority of the mean LIGS pressure values, each averaged over 50 LIGS measurements, are within one standard deviation of the mean pressure transducer data.

The LIGS pressures early in the compression stroke in the range 0.5 bar to 0.55 bar overestimate the transducer pressures of 0.44 bar by approximately 20 %. However, given the small absolute pressure difference of 0.1 bar and that the target pressure of 0.44 bar is significantly extrapolating beyond the lower limit of the calibration data (1.8 bar), this reasonable agreement indicates the re-scaled surface approach is performing robustly.

The error in LIGS derived pressure as a function of transducer pressure for the slotted piston dataset is shown in Figure 9. Due to the slow pressure rise during the first half of the compression stroke there is a very uneven distribution of pressure values, heavily weighted towards low pressures (<1 bar). Therefore for clarity, instead of sorting by transducer pressure and grouping into sets of 75 (as for Figure 7), the LIGS pressures are binned every 0.5 ± 0.25 bar in Figure 9. Despite the departure from the original calibration conditions, the mean errors of LIGS pressure measurements are below 9 % for pressures in the range 1 bar to 6.5 bar.

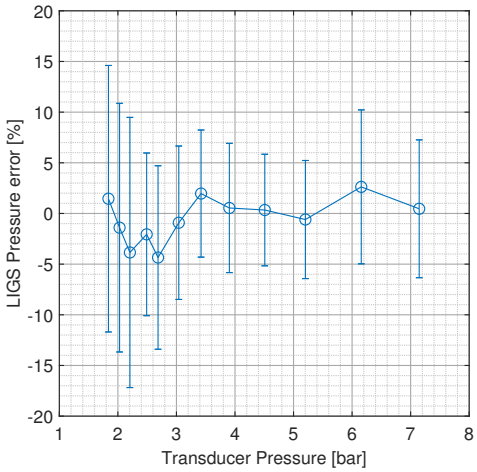

Fig. 7. Percentage errors of LIGS-derived pressure compared to transducer pressure. The LIGS 'test data' of Figure 5 is sorted by transducer pressure and divided into groups of 75 LIGS signals. Each datapoint represents the mean error and mean transducer pressure for a group of 75 LIGS signals, with errorbars corresponding to the standard deviation.

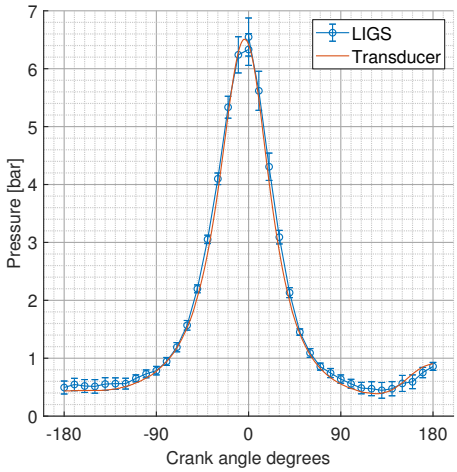

Fig. 8. LIGS-derived pressures and transducer pressures as a function of crank angle for the motored compression and expansion strokes of the optical engine. Data was obtained using a modified piston with a rectangular slot to enable measurements near TDC. Each LIGS datapoint represents the mean of pressures derived from 50 LIGS signals at a fixed crank angle, with errorbars corresponding to the standard deviation.

C. Discussion & comparison to MFM

The present results achieve comparable accuracy and precision to the Model Fitting Method of Sahlberg et al. [28] for the same slotted piston dataset (Table 1).

	Model fitting	Signal lifetime
Accuracy >1 bar	$<10\%$	$<9\%$
Precision >1 bar	$\pm$ 4 - 10%	$\pm$ 3 - 7%
Accuracy <1 bar	$<20\%$	$<25\%$
Precision <1 bar	$\pm$ 15 - 20%	$\pm$ 7 - 34%
Processing time	4 seconds	0.06 seconds
$P_{\text{reference}}$ required	single	single
Requirements	gas parameter data	calibration surface

Table 1. Comparison of pressure recovery from LIGS signals using the Model Fitting Method and the Signal Lifetime Method for the slotted piston dataset of Figure 8.

Both pressure recovery methods perform well at pressures above 1 bar, reporting LIGS pressures within 10 % of the corresponding transducer readings. The signal lifetime method shows a marginally improved precision with standard deviations for the sets of 50 LIGS pressures at each crank angle in the range 3 to 7 %, compared to between 4 and 10 % for the model fitting method. While these values also contain the cycle-to-cycle variability in the in-cylinder pressures, the fluctuations in the pressure transducer readings are approximately 1 % suggesting the dominant source of variability within the reported pressures is the uncertainty in the LIGS pressure measurement.

Below 1 bar the LIGS signals are shorter and weaker and so the decaying tail of the signal occupies a relatively smaller proportion of the signal. As a result, the effects of quenching and grating formation affect the form of the signal to a larger extent and this has a negative impact on both the MFM and the signal lifetime method, reported here, because both methods rely upon these effects having little impact on the tail of the signal that determines the accuracy of the extracted pressure measurement. While the mean error and variability in absolute terms remain similar, each approximately 0.1 bar, the relative values increase significantly due to the lower pressures involved. Below 1 bar the errors in the mean LIGS pressures are below 25 % for both methods with standard deviations up to 20 % for the model fitting method and up to 34 % for the signal lifetime method. Additionally, the signal lifetime method requires sufficient visible oscillations in the LIGS signal to accurately derive a temperature measurement for conversion of τ_{signal} to pressure via the calibration surface. As shown in Figure 9, the variability of signal lifetime-derived LIGS pressures significantly increases for pressures below 1 bar, in part due to the reduction in temperature measurement precision for these LIGS signals with typically only 3 visible oscillations.

The Model Fitting Method, MFM, [28] nominally enables pressure measurements without relying on preliminary measurements under known conditions. This MFM method does, however, require calibration using known parameters under at least a single condition in order to constrain the possible values for the rates of the 'fast' and 'slow' quenching processes and the branching ratio between them. As such, once the original calibration surface is calculated, the prior knowledge requirements for the present work – the signal lifetime method, and for the MFM are equivalent, since both require measurements under one known pressure condition.

One of the key advantages of the signal lifetime method is the rapid determination of pressure from LIGS signals. The multiple fitting steps involved in the MFM result in a processing time per measurement of approximately 4 seconds. In contrast the derivation of pressure from a LIGS signal using the signal lifetime method (derivation of temperature, calculation of τ_{signal} then application of the calibration surface) takes only 0.06 seconds

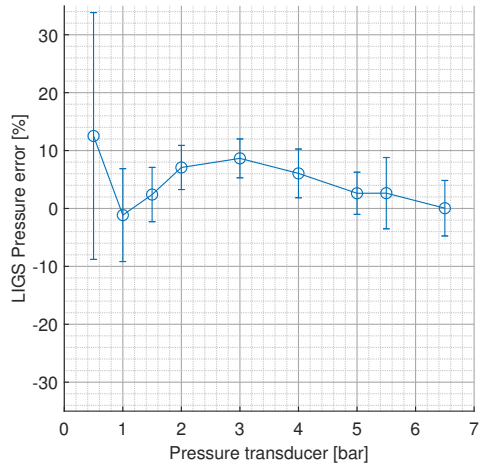

Fig. 9. Percentage errors of LIGS-derived pressures compared to transducer pressure for the slotted piston data. The LIGS data of Figure 8 is binned every 0.5 ± 0.25 bar. Each datapoint represents the mean error for the LIGS signals within each bin, with errorbars corresponding to the standard deviation.

on a laptop computer (Intel Core i7-8665U). This corresponds to a pressure readout rate of up to 16 Hz, in principle enabling readily achievable real-time measurement of both pressure and temperature using LIGS. However, data analysis remains the rate limiting step for LIGS systems with higher repetition rate pump lasers. With code optimisation and hardware improvements to reduce the time taken to perform the FFT-based temperature measurement, higher repetition rates would be feasible. A factor of 60 increase in processing speed over this work would be required to achieve 'real-time' measurement for 1 kHz LIGS measurements under diesel engine conditions [44].

6. CONCLUSIONS

A novel and rapid method to recover pressure measurement from laser-induced grating scattering (LIGS) signals has been demonstrated using data acquired from an optically-accessible single cylinder engine.

A pressure-dependent 'signal decay lifetime' was extracted from LIGS signals recorded under various engine operating conditions. Using a model based on the effect of pressure and temperature on LIGS signal decay lifetime, a calibration surface was generated relating transducer-based pressure measurements and LIGS derived temperatures to the measured LIGS signal decay lifetimes from a sparse subset of the data. For the data not used to create this calibration surface, the LIGS-based pressure recovery had a mean absolute error of $-0.5\,\%$ when compared with transducer measurements and the errors showed no discernible trend with either signal-to-noise ratio or pressure.

The portability of the calibration surface and its extrapolation has been demonstrated by applying the method to data acquired previously, over a wider range of pressures and temperatures, from transducer measurements and data acquired simultaneously using a different optical LIGS system, which used a different grating spacing. The signal lifetime method of this work was able to measure pressure to an equivalent degree of accuracy (9 %) and precision (3 % to 7 %) to the existing model fitting method for pressures above 1 bar. Translation of the calibration surface, for signal decay lifetime as a function of pressure and measured temperature, for use with different instruments required only comparison of data obtained at a single reference point, in this case, one corresponding to atmospheric conditions of temperature and pressure. Extrapolation of the calibration surface was possible due to the physics-based model defining the shape of the calibration surface, enabling pressure measurements as low as 0.5 bar, albeit at a reduced accuracy of 25 %, which is comparable to the accuracy of the model fitting method for pressures under 1 bar (20 %). It should be noted that the shape of the calibration surface is expected to be dependent on the tracer species (since this affects the photophysics of grating formation) and the gas composition.

While collimated beams were used in this work, the signal lifetime method is also applicable to focused beam geometries. The limiting factor would be the generation of a sufficiently wide grating such that the transit of the acoustic waves out of the interaction region causes minimal additional decay of the signal oscillations, enabling an accurate temperature measurement. In principle the decay of signals from electrostrictive gratings would allow a pressure measurement to be derived but would require a different analysis which is beyond the scope of this paper.

Currently the signal lifetime method represents a 60-fold reduction in processing time compared to the model fitting method, at 0.06 seconds per measurement. This provides an opportunity for simultaneous real-time pressure and temperature measurement at rates of over 10 Hz, potentially higher with further development. The pressure accuracy determined in this work is competitive with literature values for other diagnostics. In comparison to CARS in particular, it is noted that LIGS is a complementary approach since it achieves best results at super-atmospheric pressures. Collisional dephasing has a pressure-dependent influence on the CARS spectra which must be either modelled, a complex matter compared to the modelling or signal analysis required for LIGS, or minimised via the use of short pulse (fs) lasers.

Future application of the LIGS signal lifetime method for pressure recovery could be combined with other one-dimensional LIGS measurement techniques to carry out spatially-resolved optical pressure measurements, for example, measuring the propagation of a disturbance in a combustion chamber or other complex flow field.

Funding. This work was part funded by the Engineering and Physical Sciences Research Council (UK) under grant number EP/M009424/1.

Acknowledgments. The authors thank Richard Stone for help running the optical engine and Joe Camm for design of the slotted piston. An initial version of the LIGS pressure recovery algorithm described in this paper was generated as a result of a contract with Dantec Dynamics A/S. The authors are grateful for support from Jaguar Land Rover Ltd.

Disclosures. The authors declare no conflicts of interest.

Data availability. Data underlying the results presented in this paper are not publicly available at this time but may be obtained from the authors upon reasonable request.

REFERENCES

1. J. W. Gregory, K. Asai, M. Kameda, T. Liu, and J. P. Sullivan, "A review of pressure-sensitive paint for high-speed and unsteady aerodynamics," Proc. Inst. Mech. Eng. Part G: J. Aerosp. Eng. **222**, 249–290 (2008).
2. M. Semper, B. Pruski, and R. Bowersox, "Freestream turbulence measurements in a continuously variable hypersonic wind tunnel," in *50th*

AIAA Aerospace Sciences Meeting including the New Horizons Forum and Aerospace Exposition, (2012), p. 732.
3. R. K. Hanson and D. Baganoff, "Shock-tube study of nitrogen dissociation rates using pressure measurements," AIAA J. **10**, 211–215 (1972).
4. C. A. Amann, "Cylinder-pressure measurement and its use in engine research," SAE transactions pp. 418–435 (1985).
5. J. Van der Kindere, A. Laskari, B. Ganapathisubramani, and R. De Kat, "Pressure from 2D snapshot PIV," Exp. Fluids **60**, 32 (2019).
6. R. De Kat and B. Van Oudheusden, "Instantaneous planar pressure determination from piv in turbulent flow," Exp. fluids **52**, 1089–1106 (2012).
7. D. Ragni, B. W. van Oudheusden, and F. Scarano, "3D pressure imaging of an aircraft propeller blade-tip flow by phase-locked stereoscopic PIV," Exp. Fluids **52**, 463–477 (2012).
8. Y. J. Jeon, G. Gomit, T. Earl, L. Chatellier, and L. David, "Sequential least-square reconstruction of instantaneous pressure field around a body from TR-PIV," Exp. Fluids **59** (2018).
9. J. Wang, C. Zhang, and J. Katz, "GPU-based, parallel-line, omni-directional integration of measured pressure gradient field to obtain the 3D pressure distribution," Exp. Fluids **60** (2019).
10. J. D. Miller, S. Roy, J. R. Gord, and T. R. Meyer, "Communication: Time-domain measurement of high-pressure N_2 and O_2 self-broadened linewidths using hybrid femtosecond/picosecond coherent anti-Stokes Raman scattering," The J. Chem. Phys. **135**, 201104 (2011).
11. S. P. Kearney and P. M. Danehy, "Pressure measurements using hybrid femtosecond/picosecond rotational coherent anti-Stokes Raman scattering," Opt. Lett. **40**, 4082–4085 (2015).
12. M. A. Woodmansee, R. P. Lucht, and J. C. Dutton, "Development of high-resolution N_2 coherent anti-Stokes Raman scattering for measuring pressure, temperature, and density in high-speed gas flows," Appl. Opt. **39**, 6243–6256 (2000).
13. S. Roy, J. R. Gord, and A. K. Patnaik, "Recent advances in coherent anti-stokes raman scattering spectroscopy: Fundamental developments and applications in reacting flows," Prog. Energy Combust. Sci. **36**, 280 – 306 (2010).
14. R. E. Foglesong, S. M. Green, R. P. Lucht, and J. C. Dutton, "Dual-pump coherent anti-Stokes Raman scattering for simultaneous pressure/temperature measurement," AIAA J. **36**, 234–240 (1998).
15. D. Escofet-Martin, A. O. Ojo, J. Collins, N. T. Mecker, M. Linne, and B. Peterson, "Dual-probe 1D hybrid fs/ps rotational CARS for simultaneous single-shot temperature, pressure, and O_2/N_2 measurements," Opt. Lett. **45**, 4758–4761 (2020).
16. P. M. Danehy, P. H. Paul, and R. L. Farrow, "Thermal-grating contributions to degenerate four-wave mixing in nitric oxide," JOSA B **12**, 1564–1576 (1995).
17. E. Cummings, "Laser-induced thermal acoustics: simple accurate gas measurements," Opt. letters **19**, 1361–1363 (1994).
18. E. B. Cummings, I. A. Leyva, and H. G. Hornung, "Laser-induced thermal acoustics (LITA) signals from finite beams." Appl. Opt. **34**, 3290–302 (1995).
19. C. Steinhausen, V. Gerber, A. Preusche, B. Weigand, A. Dreizler, and G. Lamanna, "On the potential and challenges of laser-induced thermal acoustics for experimental investigation of macroscopic fluid phenomena," Exp. Fluids **62**, 1–16 (2020).
20. J. Kiefer and P. Ewart, "Laser diagnostics and minor species detection in combustion using resonant four-wave mixing," Prog. Energy Combust. Sci. **37**, 525–564 (2011).
21. B. Williams, M. Edwards, R. Stone, J. Williams, and P. Ewart, "High precision in-cylinder gas thermometry using laser-induced gratings: quantitative measurement of evaporative cooling with gasoline/alcohol blends in a GDI optical engine," Combust. Flame **161**, 270–279 (2014).
22. A. Stampanoni-Panariello, D. N. Kozlov, P. P. Radi, and B. Hemmerling, "Gas phase diagnostics by laser-induced gratings I. Theory," Appl. Phys. B: Lasers Opt. **81**, 101–111 (2005).
23. A. Stampanoni-Panariello, D. N. Kozlov, P. P. Radi, and B. Hemmerling, "Gas-phase diagnostics by laser-induced gratings II. Experiments," Appl. Phys. B: Lasers Opt. **81**, 113–129 (2005).
24. S. Schlamp, H. G. Hornung, T. H. Sobota, and E. B. Cummings, "Accuracy and uncertainty of single-shot, nonresonant laser-induced thermal acoustics." Appl. Opt. **39**, 5477–81 (2000).
25. R. Stevens and P. Ewart, "Single-shot measurement of temperature and pressure using laser-induced thermal gratings with a long probe pulse," App. Phys. B **78**, 111–117 (2004).
26. H. Latzel, A. Dreizler, T. Dreier, J. Heinze, M. Dillmann, W. Stricker, G. Lloyd, and P. Ewart, "Thermal grating and broadband degenerate four-wave mixing spectroscopy of OH in high-pressure flames," Appl. Phys. B **67**, 667–673 (1998).
27. R. C. Hart, G. C. Herring, and R. J. Balla, "Pressure measurement in supersonic air flow by differential absorptive laser-induced thermal acoustics," Opt. letters **32**, 1689–1691 (2007).
28. A.-L. Sahlberg, A. Luers, C. Willman, B. Williams, and P. Ewart, "Pressure measurement in combusting and non-combusting gases using laser-induced grating spectroscopy," Appl. Phys. B **125**, 46 (2019).
29. G. Hall and B. J. Whitaker, "Laser-induced grating spectroscopy," J. Chem. Soc. Faraday Transactions **90**, 1–16 (1994).
30. H. J. Eichler, P. Günter, and D. W. Pohl, "Diffraction and four-wave mixing theory," in *Laser-induced dynamic gratings,* (Springer, 1986), pp. 94–122.
31. F. De Domenico, T. F. Guiberti, S. Hochgreb, W. L. Roberts, and G. Magnotti, "Temperature and water measurements in flames using 1064 nm laser-induced grating spectroscopy (LIGS)," Combust. Flame **205**, 336 – 344 (2019).
32. B. Hemmerling, M. Neracher, D. Kozlov, W. Kwan, R. Stark, D. Klimenko, W. Clauss, and M. Oschwald, "Rocket nozzle cold-gas flow velocity measurements using laser-induced gratings," J. Raman Spectrosc. **33**, 912–918 (2002).
33. A. C. Eckbreth, "Boxcars: Crossed-beam phase-matched cars generation in gases," Appl. Phys. Lett. **32**, 421–423 (1978).
34. B. Williams, P. Ewart, X. Wang, R. Stone, H. Ma, H. Walmsley, R. Cracknell, R. Stevens, D. Richardson, H. Fu, and S. Wallace, "Quantitative planar laser-induced fluorescence imaging of multi-component fuel/air mixing in a firing gasoline-direct-injection engine: Effects of residual exhaust gas on quantitative PLIF," Combust. Flame **157**, 1866 – 1878 (2010).
35. C. Willman and P. Ewart, "Multipoint temperature measurements in gas flows using 1-D laser-induced grating scattering," Exp. Fluids **57**, 1866 – 1878 (2016).
36. P. H. Paul, R. L. Farrow, and P. M. Danehy, "Gas-phase thermal-grating contributions to four-wave mixing," JOSA B **12**, 384–392 (1995).
37. W. Hubschmid, B. Hemmerling, and A. Stampanoni-Panariello, "Rayleigh and brillouin modes in electrostrictive gratings," JOSA B **12**, 1850–1854 (1995).
38. R. Span, E. W. Lemmon, R. T. Jacobsen, W. Wagner, and A. Yokozeki, "A reference equation of state for the thermodynamic properties of nitrogen for temperatures from 63.151 to 1000 k and pressures to 2200 mpa," J. Phys. Chem. Ref. Data **29**, 1361–1433 (2000).
39. R. T. Jacobsen, R. B. Stewart, and M. Jahangiri, "Thermodynamic properties of nitrogen from the freezing line to 2000 k at pressures to 1000 mpa," J. Phys. Chem. Ref. Data **15**, 735–909 (1986).
40. E. Lemmon and S. Penoncello, "The surface tension of air and air component mixtures," in *Advances in cryogenic engineering,* (Springer, 1994), pp. 1927–1934.
41. B. A. Younglove, "Thermophysical properties of fluids. i. argon, ethylene, parahydrogen, nitrogen, nitrogen trifluoride, and oxygen," Tech. rep., NATIONAL STANDARD REFERENCE DATA SYSTEM (1982).
42. K. Stephan and A. Laesecke, "The thermal conductivity of fluid air," J. Phys. Chem. Ref. Data **14**, 227–234 (1985).
43. K. Kadoya, N. Matsunaga, and A. Nagashima, "Viscosity and thermal conductivity of dry air in the gaseous phase," J. Phys. Chem. Ref. Data **14**, 947–970 (1985).
44. F. J. Förster, C. Crua, M. Davy, and P. Ewart, "Time-resolved gas thermometry by laser-induced grating spectroscopy with a high-repetition rate laser system," Exp. Fluids **58**, 1–8 (2017).